Sigwadi et al. International Journal of Mechanical and Materials Engineering (2019) 14:2
https://doi.org/10.1186/s40712-019-0098-1

International Journal of Mechanical and Materials Engineering

ORIGINAL PAPER Open Access

Structural morphology and electronic conductivity of blended Nafion®-polyacrylonitrile/zirconium phosphate nanofibres

R. Sigwadi[1*], M. S. Dhlamini[2], T. Mokrani[1] and F. Nemavhola[3]

Abstract

This paper aimed to study the influence of zirconium phosphate (ZrP) nanoparticles on reducing the diameter of nanofibres during electrospinning. Addition of metal oxide such as zirconium phosphate decreases the diameter and smooths on the polyacrylonitrile (PAN) nanofibres as observed by the SEM techniques. Furthermore, this work investigated the effect of zirconium phosphate on the morphology and conductivity of modified PAN nanofibres under SEM, XRD and electrochemical cells. The PAN/zirconium phosphate nanofibres were obtained with the diameter ranges between 100 and 200 nm, which mean that the nanofibres morphology significantly changed with the addition of the zirconium phosphate nanoparticles. The conductivity of PAN and PAN-Nafion zirconium phosphate nanofibres was more improved when compared to that of the plain PAN nanofibres as observed under electrochemical measurements. The plain PAN nanofibres show the total degradation on thermal gravimetric analysis results when compared to the modified PAN with zirconium phosphate nanoparticles. The thermal properties and proton conductivity make the PAN/ZrP nanofibres as promising nanofillers for fuel cell electrolytes.

Keywords: Zirconium phosphate, Nanofibres, Polyacrylonitrile, Electrospinning, Electrochemical, Conductivity

Background

Polymer nanofibres are prepared by electrospinning a polymer solution, with a high-voltage electric field applied to a polymer solution ejected from a metal syringe needle. Electrospinning is when the electric forces are utilised within the polymer solution to produce the varied morphology. Moreover, by varying viscosity, surface tension, molecular structure, molecular weight, solution concentration, solvent structure, additive and operational conditions such as rotating speed, spinning head diameter, nozzle diameter and nozzle-collector distance of the same solution may produce a nanofibre web with the various fineness, orientation and surface morphology (Zhang and Lu 2014). Many researchers focus on how to synthesise high surface area nanofibres (less than 1000 nm), which make them useful in fuel cell membranes, tissue engineering, catalysis, sensors, separations, electrochemical cells, drug delivery and chemical filtration (Choi et al. 2008). Some of the researchers also focus on the proton conductivity of electrospun nanofibrous mats (Choi et al. 2008). Nafion® membrane is a perfluorinated state-of-the-art polymer developed by DuPont in the 1970s. Nafion® at low temperature maintained a high proton conductivity and chemical resistance due to its hydrophobic tetrafluoroethylene backbone and sulfonate groups. Electrospinning Nafion® solution increases the proton conductivity of nanofibres with the reduced nanometre scale (Dong et al. 2010). Electrospinning the plain Nafion® solution is impossible due to the low shear viscosity that makes Nafion® aggregates in the solution (Tran and Kalra 2013; Zhou et al. 2010). Nafion® solution was blended with other polymers such as poly(ethylene oxide) (PEO) (Ballengee and Pintauro 2011), poly(acrylic) (PAA) (Mauritz and Moore 2004), or poly(vinylalcohol) (PVA) (Chraska et al. 2000) and polyacrylonitrile (PAN) (Tran and Kalra 2013; Sharma et al. 2014) in order to enhance the mechanical

* Correspondence: sigwara@unisa.ac.za
[1]Department of Chemical Engineering, University of South Africa, Private Bag X6, Florida 1710, South Africa
Full list of author information is available at the end of the article

properties and electrospinning. Furthermore, blending Nafion® solution with electron-conducting polymers may enhance their protons' conductivity and their electrons. PAN is mostly the chosen copolymer for the preparation of fibrous filter media as it can be fabricated easily into nanofibres by electrospinning due to their superior mechanical properties, excellent weatherability and chemical stability (Nie et al. 2013). Moreover, PAN also maintains a good thermal stability at a higher temperature of 130 °C and has a good resistance to many organic solvents. PAN has been studied as a separator material, and PAN-based separators show promising properties, including high ionic conductivity, good thermal stability, high electrolyte uptake and good compatibility, with lithium metal (Gopalan et al. 2008). Electrospinning of composited PAN nanofibres has been found to have multifaceted applications (Sahay et al. 2012), such as electrode materials in supercapacitors and fuel cells (Kim et al. 2004). Zirconium oxide (ZrO_2) has several properties that make it a useful material. These properties include high density, hardness, electrical conductivity, wear resistance, high fracture toughness, low thermal conductivity and relatively high dielectric constant. Because of its high refractive index and high oxygen-ion conduction, ZrO_2 has been applied as resistive heating elements, oxygen sensors, catalysts and fuel cells (Chraska et al. 2000). The use of a totally stabilised zirconia in fuel-cell technology obtains a good ionic conductivity of cubic zirconia at medium and high temperatures (Jones and Rozière 2001). Zirconium phosphates (ZrPs) are inorganic cation-exchange material with high thermal stability. Zirconium phosphate has the features of increasing conductivity due to high proton mobility on the surface of its particles and good water retention. The reduced methanol permeability of the polymer membrane, while maintaining a high power density, is obtained by impregnating it with zirconium phosphate (Jones and Rozière 2001; Carriere et al. 2003). In this work, we study the effect of ZrP nanofillers on the improvement of the morphology and conductivity of blended Nafion®-PAN nanofibres compared with pure PAN nanofibres, which can be fabricated by electrospinning into nanofibre mats.

Methods

Materials

Nafion® solution D521 (Ion Power) was purchased from Ion Power. Polyacrylonitrile (PAN), average Mw 150,000 g/mol, was purchased from Sigma-Aldrich. N, N-dimet hylformamide (DMF) (99.8%) (Merck), sodium hydroxide (Merck), phosphoric acid (Merck), sulphuric acid (Merck), zirconium oxychloride hydrate (Merck) and potassium chloride (KCl) were obtained and used as received.

Preparation of electrospinning solutions

Plain polyacrylonitrile (PAN) nanofibre solutions were obtained by dissolving PAN (1 g) in DMF (6 g) solution, and a magnetic mixer stirred the solutions for 3 h at 80 °C (Pilehrood et al. 2012). The obtained solution was divided into three parts. One part was for plain PAN, and other parts were for the PAN/ZrP and Nafion®-PAN/ZrP nanofibres as shown in Fig. 1. In order to prepare the PAN/ZrP nanofibres, 0.1 wt% ZrP nanoparticles were added to the obtained solution and sonicated for 30 min to obtain a homogenous solution and magnetically stirred for 3 h at 80 °C. Moreover, the third part, 5:5 Nafion®/PAN and 0.1 wt% ZrP nanoparticles were added and magnetically stirred for 3 h at 80 °C. The obtained solution was spun by an electrospinning system perpendicularly aligned to the target collector. The electrospinning solution was fed by using a syringe of 10 mL through a capillary tip with a diameter of 1.25 mm. The following electrospinning parameters have been used in order to reduce the diameter of the nanofibres into nano range. A voltage of 16 kV and a syringe pump were used to feed the electrospinning solution at a constant rate of 0.5 mL/h. The distance between the needletip and the

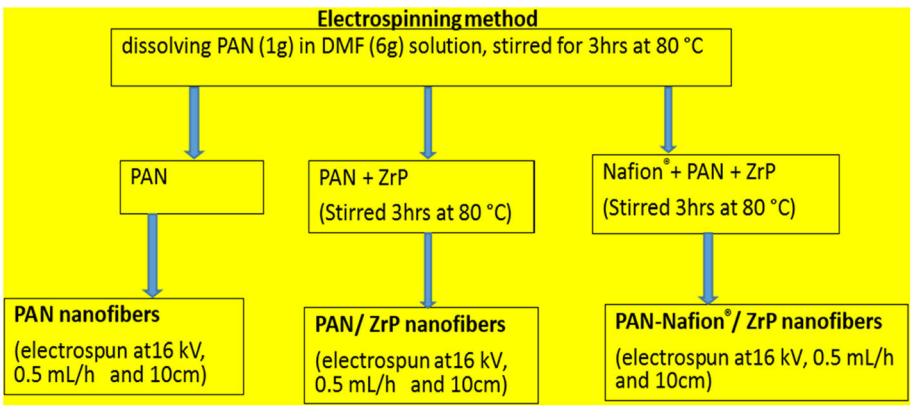

Fig. 1 Electrospinning process

collector was set as 10 cm. The collector plate was covered with aluminium foil to gather the resultant nanofibres at a specified distance.

Characterisation

The XRD analysis was performed using a Philips X-ray automated diffractometer, with a Cu K radiation source. Samples were scanned in continuous mode, from 5° to 90° (2θ). The thermal properties of the samples and their characteristics were studied by thermal gravimetric analysis (TGA) under nitrogen flow. TGA data was obtained with the PerkinElmer instrument, over nitrogen and at a heating rate of 10 °C/min from 50 to 1000 °C. Fourier transform infrared (FTIR) spectroscopy was used to determine the quality and composition of the sample. FTIR spectra were obtained with a (Vertex 70 Bruker) FTIR instrument over a range of 4000–400 cm^{-1} and a resolution of 4 cm^{-1}. The surface morphology of the nanofibres was analysed by atomic force microscopy (AFM) and scanning microscopy (SEM).

Electrochemical studies

Electrochemical measurements were observed under three electrodes. While a silver-silver chloride (Ag/AgCl) electrode was used as the reference electrode (Anand et al.

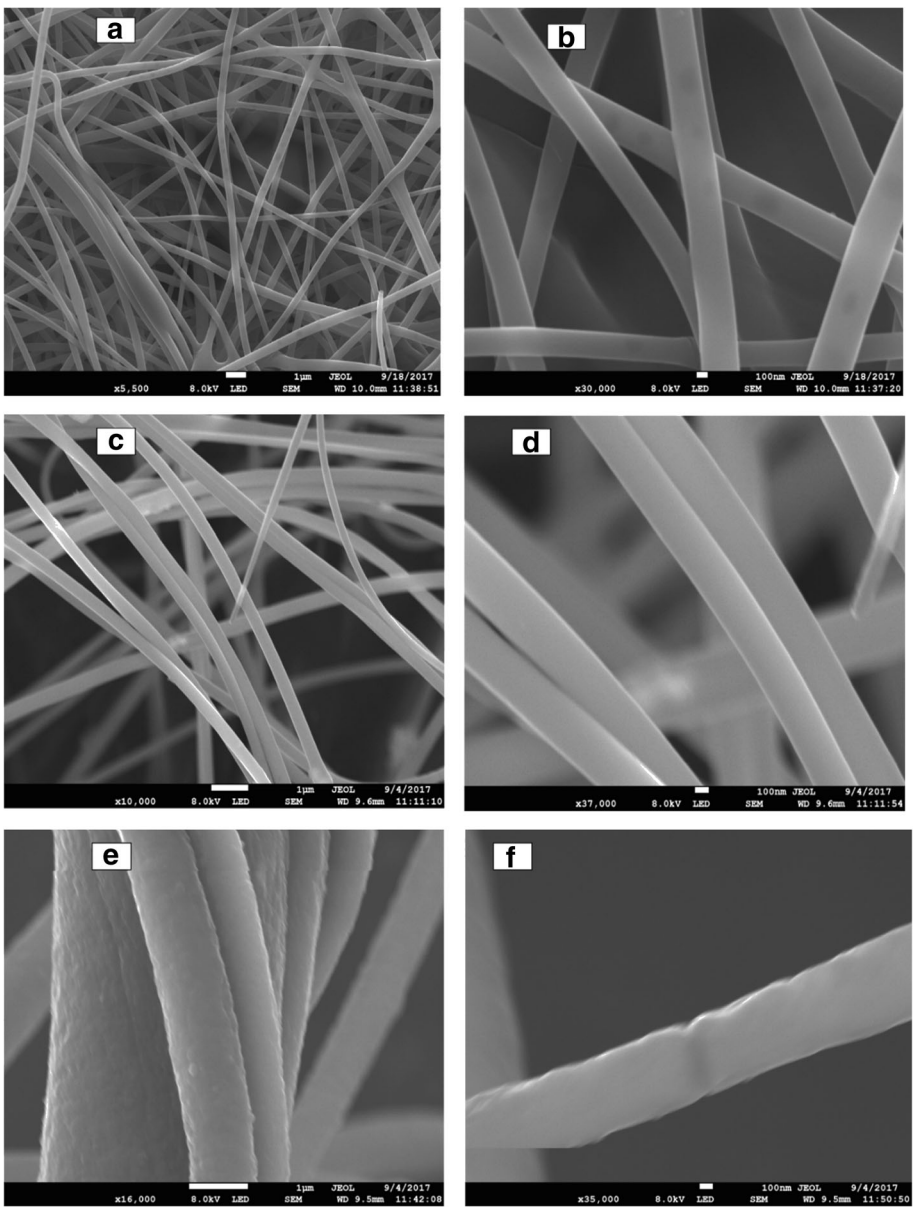

Fig. 2 Scanning electron microscopy (SEM). **a** and **b** SEM micrographs of PAN nanofibres. **c** and **d** micrographs of PAN/ZrP nanofibres. **e** and **f** micrographs of PAN-Nafion/ZrP nanofibres at low and high magnification

2014), zirconium nanoparticles coated on glassy carbon were used as a working electrode, and Pt wire was used as a counter electrode. 0.03 g of PAN, PAN/ZrP and Nafion®-PAN/ZrP nanofibres were ultra-onicated in 0.5 mL of 1 wt% Nafion® in absolute ethanol for 30 min, pipetted a 0.05 mL suspension onto the glassy carbon electrode, and dried at ambient temperature (Dong et al. 2009). Cyclic voltammetry (CV) and electrochemical impedance spectroscopy (EIS) were observed under 2 M of KCl electrolyte. The scan rates used were 10 mV s^{-1}, 20 mV s^{-1}, 30 mV s^{-1}, 50 mV s^{-1} and 100 mV s^{-1} with the CV test ranging from − 0.15 to 0.55 V vs. EIS measurements were obtained under the frequency range of 100 kHz to 0.01 Hz.

Results and discussion

Morphologies and structures

The effect of zirconium phosphate nanoparticles on nanofibres were confirmed under SEM micrographs of PAN, PAN/ZrP and PAN-Nafion®/ZrP nanofibres electrospun on the same conditions (voltage 16 kV, distance 10 mm) as presented in Fig. 2. It was observable in Fig. 2a–b that nanofibres are smooth, uniform in morphologies and uniformly arranged on top of each other with average diameters of 100–200 nm. The modified PAN nanofibres with zirconium phosphate nanoparticles showed the surface smoothness with the reduced diameters of 100–150 nm as presented in Fig. 2c–d. These may be due to the increase of conductivity within the composited solution with zirconium phosphates ions, which reduced the diameter of the nanofibres (Nayak et al. 2012). At a lower magnification of 100 nm, PAN/ ZrP nanofibres present smooth and overlaying on top of each other; this could be due to the presence of zirconium phosphate nanoparticles within the nanofibres as shown in Figs. 2d and 3d. Figure 1e–f shows that PAN-Nafion®/ZrP nanofibres obtained a different mor phology with the rougher surface without beads and slightly

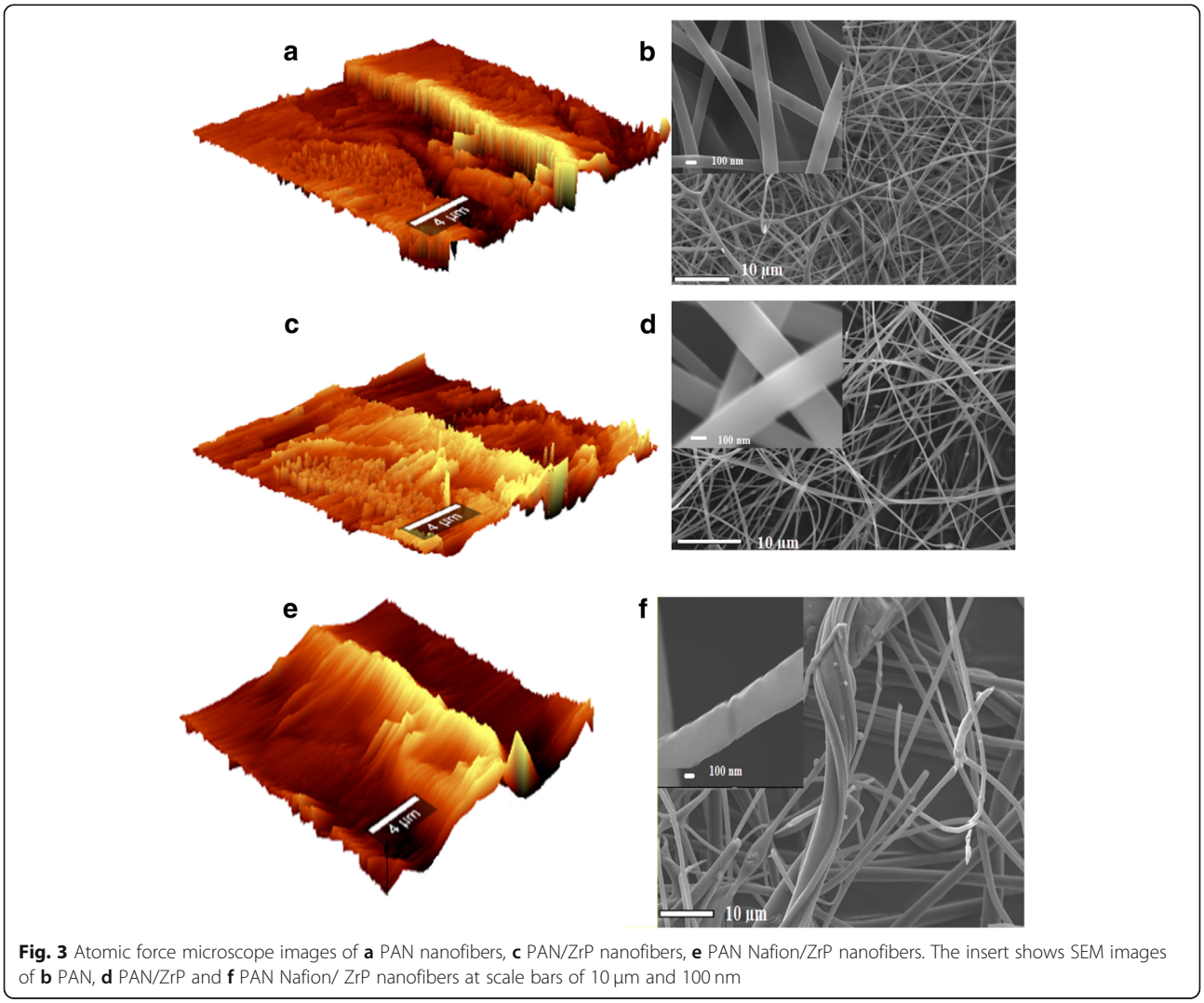

Fig. 3 Atomic force microscope images of **a** PAN nanofibers, **c** PAN/ZrP nanofibers, **e** PAN Nafion/ZrP nanofibers. The insert shows SEM images of **b** PAN, **d** PAN/ZrP and **f** PAN Nafion/ ZrP nanofibers at scale bars of 10 µm and 100 nm

increases diameters of 150–300 nm whereas the PAN nanofibres obtained a uniform morphology and relatively smoother surface (Fong et al. 1999). That surface roughness and slightly increased diameter may be due to the addition of a Nafion® solution (Sharma et al. 2014). Furthermore, the addition of ZrP nanoparticles in the PAN-Nafion® solution reduces the diameters as presented in Figs. 2e–f and 3f. Topography images measured in tapping mode of PAN, PAN/ZrP and PAN-Nafion®/ZrP nanofibres are shown in Fig. 3. Figure 3c shows that the PAN-Nafion® solution modified with ZrP nanoparticles has roughness in all the area, when compared with PAN/ZrP (Fig. 3b) and PAN (Fig. 3a) nanofibres, which shows less roughness in all the dark (hydrophilic) and light (hydrophobic) sections (Shin et al. 2014). This may be due to the Nafion® solution that introduced the surface roughness of nanofibres. Moreover, PAN-Nafion®/ZrP nanofibres have more darkness than the lighter surface; these may be due to the enhanced water within the nanofibres.

The X-ray diffraction (XRD) analysis

Figure 4 shows the X-ray diffraction pattern of PAN, PAN/ZrP and PAN-Nafion®/ZrP nanofibres. The weak peak at $2\theta = 17.6°$, $2\theta = 24.9°$, $2\theta = 37.1°$, $2\theta = 50.4°$, $2\theta = 55.4°$ and $2\theta = 59.1°$, with a strong peak of $2\theta = 39.2°$, indicated the crystalline peaks of ZrP as shown in Fig. 4a. This PAN-Nafion®/ZrP nanofibres show that peaks at 2θ are 21.5°, 26.8°, 30.8°, 36.4°, 49.4°, 54.5° and 58.1° which correspond to planes (2 0 0), (2 1 1), (2 2 0), (3 1 1), (4 2 0) as shown in Fig. 4b (Trobajo et al. 2000; Zhao et al. 2005). XRD patterns in Fig. 4b show only the crystalline peak of ZrP nanoparticles without reflecting the peak of electrospun Nafion® and PAN. Appearance of ZrP crystalline peaks indicates that the metal oxide was successfully composited within the electrospun nanofibres. The PAN nanofibres are amorphous with the strong peak at $2\theta = 17.6°$ that assigned to crystal planes of PAN as shown in Fig. 4c (Mathur et al. 1991).

Fourier transform infrared spectroscopy (FTIR)

FTIR spectra analysis of PAN, PAN/ZrP and PAN-Nafion/ZrP nanofibres is presented in Fig. 5. Figure 5a–c shows the vibration peak at 2933 cm^{-1} (CH stretching) and 1456 cm^{-1} (CH bending) which can be assigned to vibrations of the CH and CH_2 group of PAN (Zhang et al. 2010). Also, the peaks at 2246 cm^{-1}, 1673 cm^{-1} and 1630 cm^{-1} related to the stretching vibration of nitrile groups C≡N and C=O stretching vibrations of the acrylonitrile (Neghlani et al. 2011). Figure 5a shows the vibration peaks of 1097 cm^{-1} and 658 cm^{-1} that are assigned to Zr–O vibration and P–O_4 stretching due to the presence of ZrP nanoparticles within the PAN nanofibres and 978 cm^{-1} which correspond to the C–O–C stretching (Jansen and Guenther 1995). FTIR spectrum of the composite PAN-Nafion/ZrP nanofibres shows the presence of Nafion polymer (Salavati-Niasari et al. 2009) as shown in Fig. 5b, with the strong bands at 1233 cm^{-1} and 1149 cm^{-1}, which correspond to the –C–F– stretching (Ostrowska and Narebska 1983; Zhai et al. 2006). Figure 5a–b shows the disappearance of vibrational structures at 1742 cm^{-1} for C=O stretching vibration of the PAN backbone (Di Noto et al. 2006). This may be due to the incorporation of ZrP

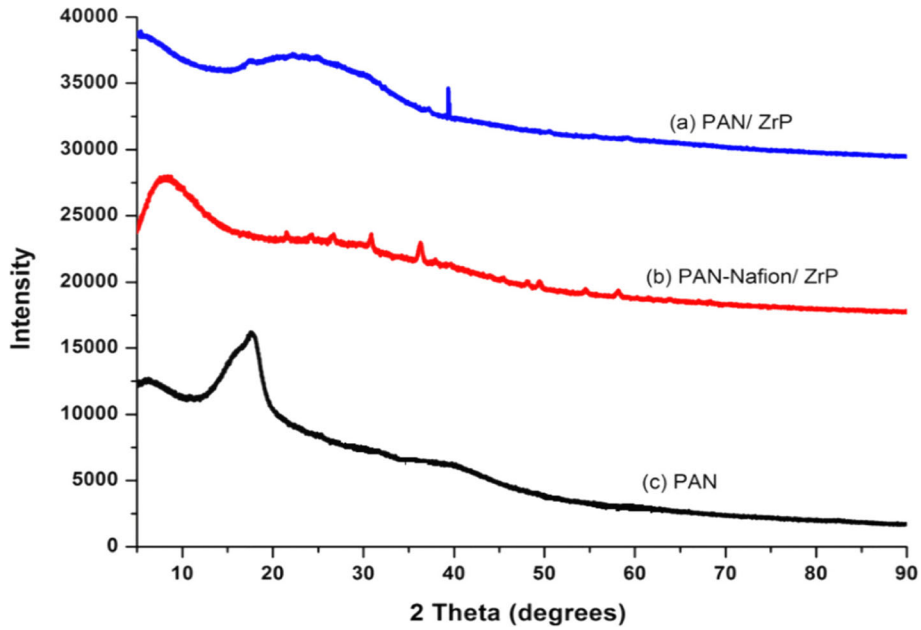

Fig. 4 The comparison of the XRD patterns of the **a** PAN/ZrP nanofibres, **b** PAN-Nafion®/ZrP nanofibres and **c** PAN nanofibres

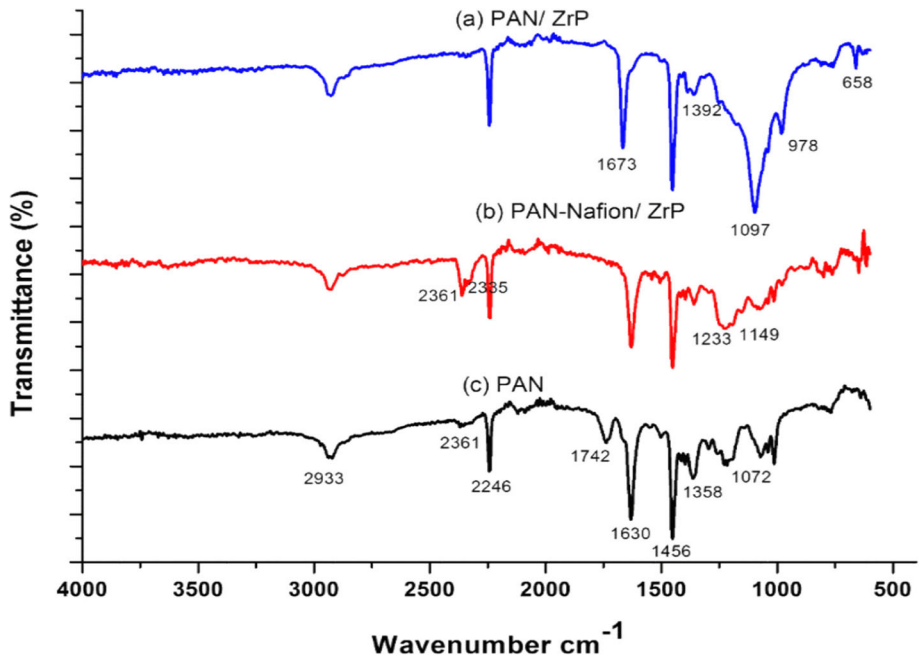

Fig. 5 FTIR spectra of **a** PAN/ZrP nanofibres, **b** PAN-Nafion/ZrP nanofibres and **c** PAN nanofibres

nanoparticles that reduced some of the vibration peaks of PAN polymer. Figure 5a–b shows vibration bands at 2361 cm^{-1} which are assigned to O–H bonding, and the peak observed at 2335 cm^{-1} is due to the presence of inorganic ions. Therefore, the appearance of Zr–O groups at the PAN nanofibres was caused by the zirconium phosphates composited within the electrospun solution.

Thermo-gravimetric analysis (TGA) and derivative thermo-gravimetric

Figure 6 shows the TGA curve of PAN nanofibres with derivative thermo-gravimetric (DTG) curve in the insert. The TGA results show that the initial weight loss occurred at 150 °C in PAN-Nafion/ZrP nanofibres, with a little weight loss as shown in Fig. 6A (a) due to dehydration. The

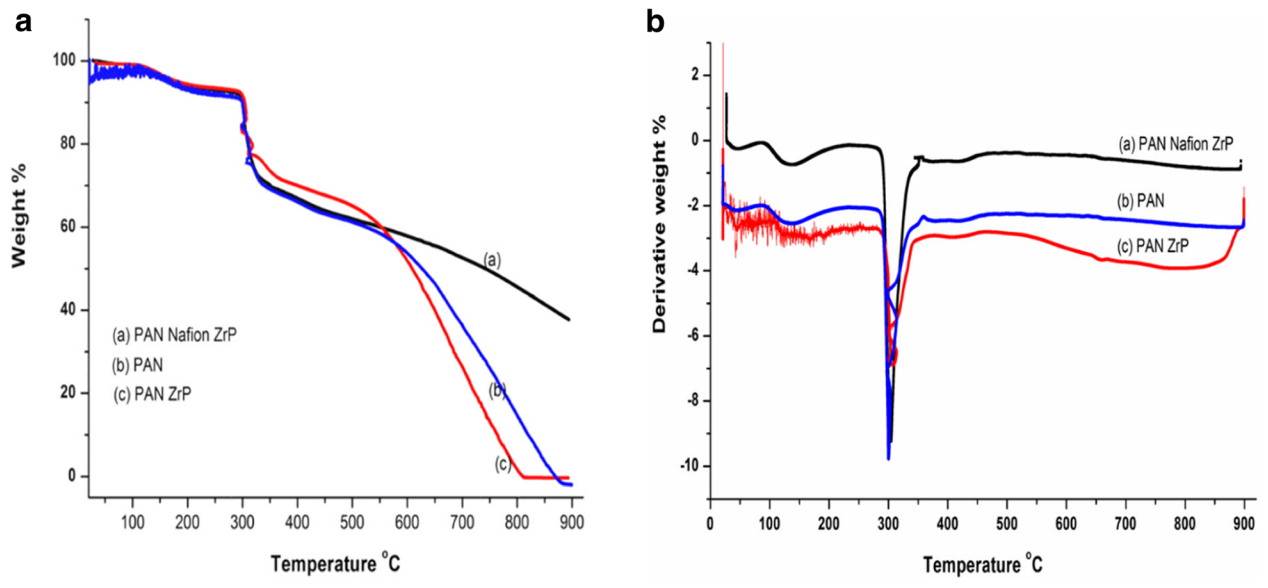

Fig. 6 a The thermal gravimetric analysis (TGA) and **b** derivative thermogravimetric (DTG) analysis of (**a**) PAN-Nafion/ZrP nanofibers, (**b**) PAN nanofibers and (**c**) PAN/ZrP nanofibers

second weight loss occurs at 333 °C, due to the release of the volatile gases (Alarifi et al. 2015). The third weight loss occurs at 565 °C, due to partial evaporation of NH_3 and HCN (Ouyang et al. 2008). Figure 6A (a) shows that PAN-Nafion/ZrP nanofibres are thermally more stable than PAN and PAN/ZrP nanofibres as they have a higher decomposition temperature. These may be due to thermal decomposition of composited Nafion polymer that occurs in three stages and the incorporation of ZrP nanoparticles that presented the interactions between ZrP and Nafion-PAN nanofibres. Figure 6A (b) show that PAN nanofibres' initial weight loss occurs at 150 °C, and the second weight loss occurs at 333 °C, due to the release of the volatile gases (Alarifi et al. 2015). The third weight loss occurs at 565 °C, due to partial evaporation of NH_3 and HCN (Ouyang et al. 2008). In addition, the final weight loss stage is at 882 °C, due to the total evaporation of polymer chain fragments from the PAN nanofibres. The DTG of PAN-Nafion/ZrP nanofibres, PAN nanofibres and PAN/ZrP nanofibres shows a weight above 300 °C as shown in the Fig. 6B, which shows the thermal stability of the electrospun nanofibres. Figure. 6B (c) shows only one peak; this may be due to the addition of ZrP nanoparticles within the PAN

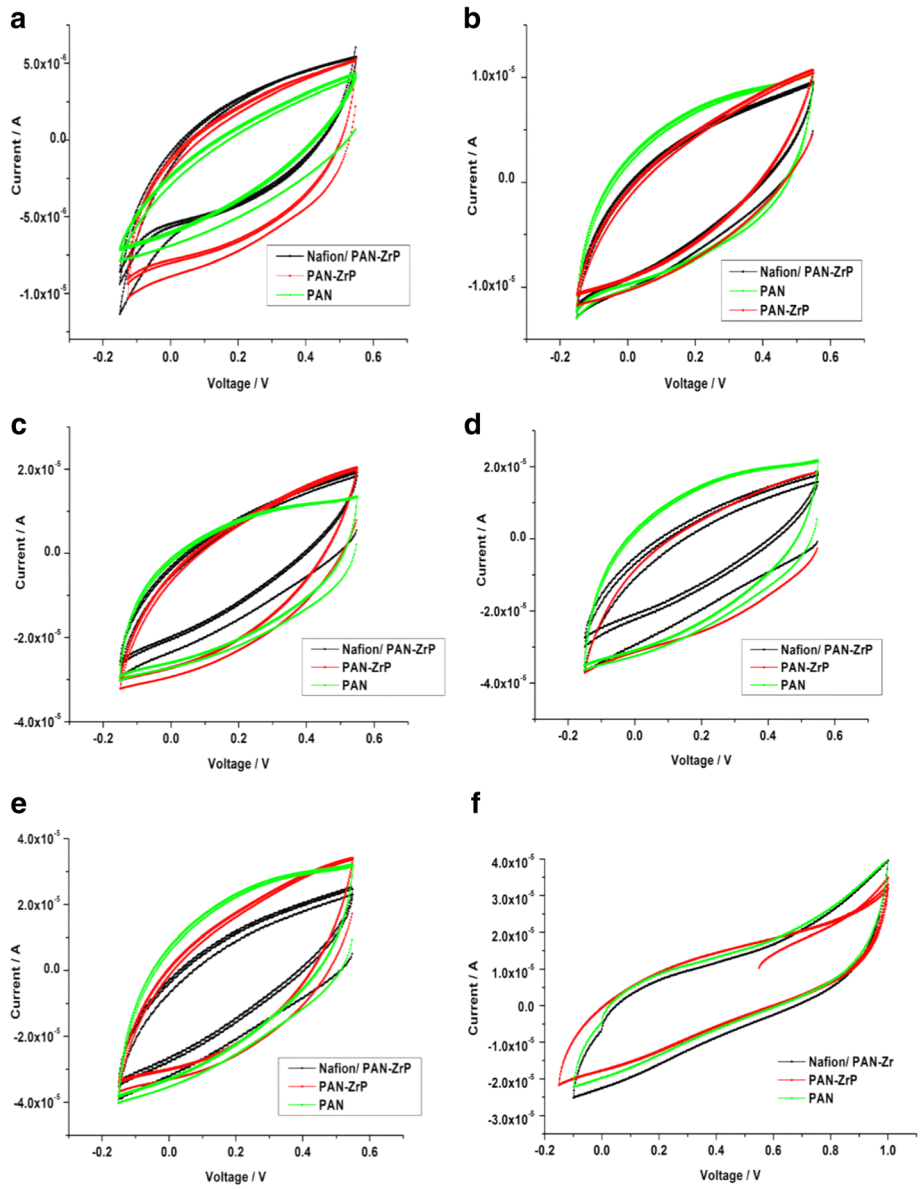

Fig. 7 Cyclic voltammogrammes of PAN, PAN/ZrP and PAN-Nafion/ZrP nanofibres at **a** 10 mV s^{-1}, **b** 20 mV s^{-1}, **c** 30 mV s^{-1}, **d** 50 mV s^{-1}, **e** 100 mV s^{-1} and **f** 100 mV s^{-1} and CV test ranging from − 0.15 to 1.0 V

nanofibres, which stabilised the weight loss peak. The DTG weight loss peak at around 600–850 °C can be due to nitrile groups' degradation.

Electrochemical properties

Figure 7 shows the cyclic voltammogrammes (CV) of PAN, PAN/ZrP and PAN-Nafion/ZrP nanofibres at a scan rate of 10 mV s^{-1}, 20 mV s^{-1}, 30 mV s^{-1}, 50 mV s^{-1} and 100 mV s^{-1}. The CV of modified PAN shows a higher current response and less estimated charge transfer resistance in all the scanning rates as shown in Fig. 7a–f. In Fig. 7a–f, it is observed that the current is directly proportional to the scan rates of CV, as when the scan rate increases, the current also increases (Nguyen et al. 2015). This may be due to the higher response of redox peak in all the nanofibres. Figure 7f shows the electrochemical stability of all the nanofibres at the scan rate of 100 mV s^{-1} and 5 cycles, with CV test ranging from − 0.15 to 1.0 V, as it has obtained a rectangular curve at high electronic conductivity and good charge dissemination (Babakhani and Ivey 2010). This indicates that these nanofibres can be suitable materials to be used as electrolytes or the modification of electrolytes for the application of supercapacitors (Zhang and Zhao 2009) or fuel cells due to their fast charge and discharge behaviour. However, the CV reduction of PAN-Nafion/ZrP nanofibres at a scan rate of 10 mV s^{-1}, 20 mV s^{-1}, 30 mV s^{-1}, 50 mV s^{-1} and 100 mV s^{-1} may be due to the conductivity as confirmed by Nyquist plots below. Figure 8a and b shows the Nyquist plots of PAN,

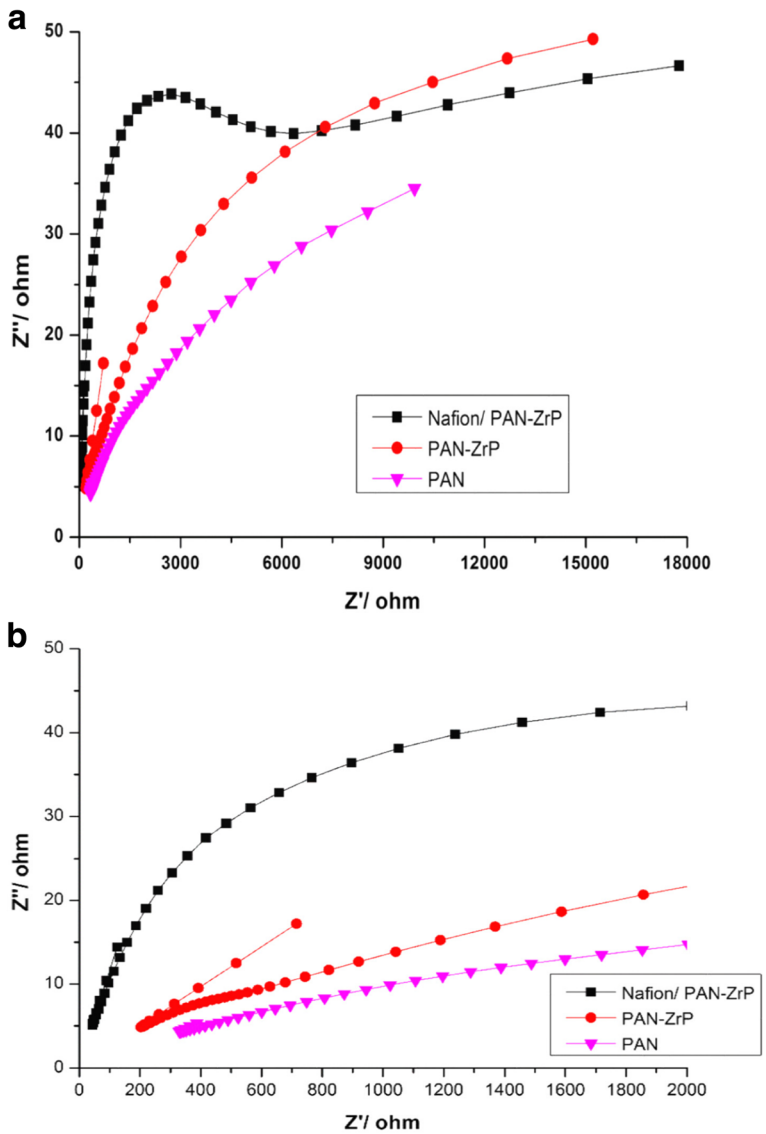

Fig. 8 Nyquist plots for PAN, PAN/ ZrP and PAN-Nafion/ ZrP nanofibers **a** at low frequencies and **b** at high frequencies

PAN/ZrP and PAN-Nafion/ZrP nanofibres. It can be observed in Fig. 8a and b that PAN-Nafion/ZrP nanofibres obtained a nearly straight line without a semicircle in the high-frequency region. This indicates the ultralow charge transfer resistance during the electro-catalytic process in the composite nanofibres. Figure 8b shows that PAN/ZrP and PAN-Nafion/ZrP nanofibres obtained a smaller resistance when compared with that of plain PAN nanofibres. These may be due to the incorporation of a ZrP nanoparticle, which has high proton mobility. However, PAN-Nafion/ZrP nanofibres show as highly conductive as they can be observed on Nyquist plots as show in Fig. 8a, which obtained a very steep line that shows how fast the charge transfers (Kim and Yang 2014). PAN/ZrP nanofibres show steep linear slopes at high frequencies as presented in Fig. 8a. It is observable that the conductivity for PAN-Nafion/ZrP and PAN/ZrP nanofibres is more improved than the plain PAN nanofibres. This shows that the addition of the ZrP nanoparticle has an impact on increasing electro-catalytic resistance. Furthermore, the plain PAN nanofibres show a long arc in the high-frequency region and a relatively flat curve in the low-frequency region, due to its poor electroactivity in charge transport, compared with the modified PAN nanofibres as shown in Fig. 8b.

Conclusion

The SEM images show that the electrospun PAN-Nafion nanofibres modified by ZrP nanoparticles obtained a reduced diameter and roughness without the formation of beads. In addition, PAN shows a more reduced diameter of 100 nm due to the ZrP nanoparticles being well distributed within the nanofibres. The XRD results also show well-crystallised zirconium phosphates within the modified PAN nanofibres. Moreover, the obtained results show that the thermal degradation properties of PAN-Nafion/ZrP nanofibres improve at a high temperature of 500 °C and with a high conductivity under CV and Nyquist plots. It can be concluded that the addition of ZrP nanoparticles within PAN and PAN/Nafion nanofibres can reduce the diameter while improving the conductivity. When PAN is blended with Nafion solution, it stabilised the high decomposition temperature of Nafion. Furthermore, PAN-Nafion/ZrP nanofibres show a high stability in Nyquist plots due to the incorporation of zirconium phosphate nanoparticles that allow improved electrode surface accessibility. The plots obtained rectangular curves at high electronic conductivity and good charge dissemination. This makes composited nanofibres with ZrP nanoparticles suitable to be used as the electrolyte of a promising fuel cell application.

Abbreviations

AFM: Atomic force microscopy; Ag/AgCl: Silver-silver chloride; CV: Cyclic voltammetry; DMF: N, N-dimethylformamide; EIS: Electrochemical impedance spectroscopy; FTIR: Fourier transform infrared; KCl: Potassium chloride; PAA: Poly(acrylic); PAN: Polyacrylonitrile; PEO: Poly(ethylene oxide); PVA: Poly(vinylalcohol); SEM: Scanning electron microscopy; TGA: Thermal gravimetric analysis; XRD: X-ray diffraction; ZrO_2: Zirconium oxide; ZrP: Zirconium phosphate

Acknowledgements

The authors are thankful to thank UNISA for the SEM results. We also acknowledged National Research Funding (NRF) and University of South Africa (Academic Qualification Improvement Programme (AQIP)) for their financial support.

Funding

National Research Funding (NRF) (Grant UID:95333) and University of South Africa (Academic Qualification Improvement Programme (AQIP)).

Availability of data and materials

All data analysed during this study are available from the corresponding author on request.

Authors' contributions

The authors read and correct the manuscript. All authors read and approved the final manuscript.

Competing interests

The authors declare that they have no competing interests.

Publisher's Note

Author details

[1]Department of Chemical Engineering, University of South Africa, Private Bag X6, Florida 1710, South Africa. [2]Department of Physics, University of South Africa, Private Bag X6, Florida 1710, South Africa. [3]Department of Mechanical and Industrial Engineering, University of South Africa, Private Bag X6, Florida 1710, South Africa.

Received: 12 October 2018 Accepted: 4 January 2019
Published online: 23 January 2019

References

Alarifi, I. M., Alharbi, A., Khan, W. S., Swindle, A., & Asmatulu, R. (2015). Thermal, electrical and surface hydrophobic properties of electrospun polyacrylonitrile nanofibers for structural health monitoring. *Materials, 8*, 7017–7031.

Anand, T. J. S., Zaidan, M., Azam, M. A., & Buang, Z. (2014). Structural studies of NiTe 2 thin films with the influence of amino additives. *International Journal of Mechanical and Materials Engineering, 9*, 18.

Babakhani, B., & Ivey, D. G. (2010). Anodic deposition of manganese oxide electrodes with rod-like structures for application as electrochemical capacitors. *Journal of Power Sources, 195*, 2110–2117.

Ballengee, J., & Pintauro, P. (2011). Morphological control of electrospun Nafion nanofiber mats. *Journal of the Electrochemical Society, 158*, B568–B572.

Carriere, D., Moreau, M., Lhalil, K., Barboux, P., & Boilot, J. (2003). Proton conductivity of colloidal nanometric zirconium phosphates. *Solid State Ionics, 162*, 185–190.

Choi, J., Lee, K. M., Wycisk, R., Pintauro, P. N., & Mather, P. T. (2008). Nanofiber network ion-exchange membranes. *Macromolecules, 41*, 4569–4572.

Chraska, T., King, A. H., & Berndt, C. C. (2000). On the size-dependent phase transformation in nanoparticulate zirconia. *Materials Science and Engineering: A, 286*, 169–178.

Di Noto, V., Gliubizzi, R., Negro, E., & Pace, G. (2006). Effect of SiO2 on relaxation phenomena and mechanism of ion conductivity of [Nafion/(SiO2) x] composite membranes. *The Journal of Physical Chemistry B, 110*, 24972–24986.

Dong, B., Gwee, L., Salas-de la Cruz, D., Winey, K. I., & Elabd, Y. A. (2010). Super proton conductive high-purity Nafion nanofibers. *Nano Letters, 10*, 3785–3790.

Dong, W.-S., Lin, F.-Q., Liu, C.-L., & Li, M.-Y. (2009). Synthesis of ZrO2 nanowires by ionic-liquid route. *Journal of Colloid and Interface Science, 333*, 734–740.

Fong, H., Chun, I., & Reneker, D. (1999). Beaded nanofibers formed during electrospinning. *Polymer, 40*, 4585–4592.

Gopalan, A. I., Santhosh, P., Manesh, K. M., Nho, J. H., Kim, S. H., Hwang, C.-G., & Lee, K.-P. (2008). Development of electrospun PVdF–PAN membrane-based polymer electrolytes for lithium batteries. *Journal of Membrane Science, 325*, 683–690.

Jansen, M., & Guenther, E. (1995). Oxide gels and ceramics prepared by a nonhydrolytic sol-gel process. *Chemistry of Materials, 7*, 2110–2114.
Jones, D. J., & Rozière, J. (2001). Recent advances in the functionalisation of polybenzimidazole and polyetherketone for fuel cell applications. *Journal of Membrane Science, 185*, 41–58.
Kim, B.-H., & Yang, K. S. (2014). Structure and electrochemical properties of electrospun carbon fiber composites containing graphene. *Journal of Industrial and Engineering Chemistry, 20*, 3474–3479.
Kim, C., Choi, Y.-O., Lee, W.-J., & Yang, K.-S. (2004). Supercapacitor performances of activated carbon fiber webs prepared by electrospinning of PMDA-ODA poly (amic acid) solutions. *Electrochimica Acta, 50*, 883–887.
Mathur, R., Bahl, O., Mittal, J., & Nagpal, K. (1991). Structure of thermally stabilized PAN fibers. *Carbon, 29*, 1059–1061.
Mauritz, K. A., & Moore, R. B. (2004). State of understanding of Nafion. *Chemical Reviews, 104*, 4535–4586.
Nayak, R., Padhye, R., Kyratzis, I. L., Truong, Y. B., & Arnold, L. (2012). Recent advances in nanofibre fabrication techniques. *Textile Research Journal, 82*, 129–147.
Neghlani, P. K., Rafizadeh, M., & Taromi, F. A. (2011). Preparation of aminated-polyacrylonitrile nanofiber membranes for the adsorption of metal ions: comparison with microfibers. *Journal of Hazardous Materials, 186*, 182–189.
Nguyen, T., Carmezim, M. J., Boudard, M., & Montemor, M. F. (2015). Cathodic electrodeposition and electrochemical response of manganese oxide pseudocapacitor electrodes. *International Journal of Hydrogen Energy, 40*, 16355–16364.
Nie, G., Li, Z., Lu, X., Lei, J., Zhang, C., & Wang, C. (2013). Fabrication of polyacrylonitrile/CuS composite nanofibers and their recycled application in catalysis for dye degradation. *Applied Surface Science, 284*, 595–600.
Ostrowska, J., & Narebska, A. (1983). Infrared study of hydration and association of functional groups in a perfluorinated Nafion membrane, Part 1. *Colloid and Polymer Science, 261*, 93–98.
Ouyang, Q., Cheng, L., Wang, H., & Li, K. (2008). Mechanism and kinetics of the stabilization reactions of itaconic acid-modified polyacrylonitrile. *Polymer Degradation and Stability, 93*, 1415–1421.
Pilehrood, M. K., Heikkilä, P., & Harlin, A. (2012). Preparation of carbon nanotube embedded in polyacrylonitrile (pan) nanofibre composites by electrospinning process. *AUTEX Research Journal, 12*, 1–6.
Sahay, R., Kumar, P. S., Sridhar, R., Sundaramurthy, J., Venugopal, J., Mhaisalkar, S. G., & Ramakrishna, S. (2012). Electrospun composite nanofibers and their multifaceted applications. *Journal of Materials Chemistry, 22*, 12953–12971.
Salavati-Niasari, M., Dadkhah, M., & Davar, F. (2009). Pure cubic ZrO 2 nanoparticles by thermolysis of a new precursor. *Polyhedron, 28*, 3005–3009.
Sharma, D. K., Shen, J., & Li, F. (2014). Reinforcement of Nafion into polyacrylonitrile (PAN) to fabricate them into nanofiber mats by electrospinning: characterization of enhanced mechanical and adsorption properties. *RSC Advances, 4*, 39110–39117.
Shin, D. W., Lee, S. Y., Kang, N. R., Lee, K. H., Cho, D. H., Lee, M. J., Lee, Y. M., & Do Suh, K. (2014). Effect of crosslinking on the durability and electrochemical performance of sulfonated aromatic polymer membranes at elevated temperatures. *International Journal of Hydrogen Energy, 39*, 4459–4467.
Tran, C., & Kalra, V. (2013). Co-continuous nanoscale assembly of Nafion–polyacrylonitrile blends within nanofibers: a facile route to fabrication of porous nanofibers. *Soft Matter, 9*, 846–852.
Trobajo, C., Khainakov, S. A., Espina, A., & García, J. R. (2000). On the synthesis of α-zirconium phosphate. *Chemistry of Materials, 12*, 1787–1790.
Zhai, Y., Zhang, H., Hu, J., & Yi, B. (2006). Preparation and characterization of sulfated zirconia (SO42−/ZrO2)/Nafion composite membranes for PEMFC operation at high temperature/low humidity. *Journal of Membrane Science, 280*, 148–155.
Zhang, C., Yang, Q., Zhan, N., Sun, L., Wang, H., Song, Y., & Li, Y. (2010). Silver nanoparticles grown on the surface of PAN nanofiber: preparation, characterization and catalytic performance. *Colloids and Surfaces A: Physicochemical and Engineering Aspects, 362*, 58–64.
Zhang, L. L., & Zhao, X. S. (2009). Carbon-based materials as supercapacitor electrodes. *Chemical Society Reviews, 38*, 2520–2531.
Zhang, X., & Lu, Y. (2014). Centrifugal spinning: an alternative approach to fabricate nanofibers at high speed and low cost. *Polymer Reviews, 54*, 677–701.
Zhao, G., Yuan, Z., & Chen, T. (2005). Synthesis of amorphous supermicroporous zirconium phosphate materials by nonionic surfactant templating. *Materials Research Bulletin, 40*, 1922–1928.
Zhou, C., Liu, Z., Dai, J., & Xiao, D. (2010). Electrospun Ru (bpy) 32+-doped nafion nanofibers for electrochemiluminescence sensing. *Analyst, 135*, 1004–1009.